A Numerical Model of Vortex-Induced Vibration on Marine Risers

Hamed Ashuri[1], Keyvan Sadeghi[2*], Saeid Niazi[3]

[1] *MSc, Hormozgan University; Hamedashuri@gmail.com*

[2*] *Corresponding author: Assistant professor, Buein Zahra Technical University; keyvan.sadeghi@bzte.ac.ir*

[3] *Assistant professor, Hormozgan University, s.niazi@hormozgan.ac.ir*

ARTICLE INFO

ABSTRACT

The Steger and Warming flux vector splitting implicit scheme is used to numerically solve two dimensional Reynolds Averaged Navier–Stokes (RANS) equations governing the vortex induced vibration of a flexible riser laterally supported by a spring and a damper. The $k–\varepsilon$ model is used as turbulence model to simulate the turbulent flow in the wake of the riser. To update the new position of the riser, the lift coefficient obtained from the previous RANS iteration is coupled by the body motion equation. The proposed numerical solution is able to provide fair results in terms of lift coefficient, amplitude of oscillation and the effect of reduced velocity on it. The numerical results are compared with the available experimental and computational data where fairly good agreement even at the lock-in regime has been obtained. Taking wider external boundary, using conservative form of the equations, applying k-ε turbulence model for the separated flow and finally using the variable time step as the lock–in region approaches, are main features of the proposed numerical model.

1. Introduction

Vortex-induced vibration (VIV) is a vibration due to oscillatory lift force caused by alternating vortex shedding from opposite sides of slender bluff bodies. VIV can have damaging effects on structures when the frequency of vortex shedding is in vicinity of one of the natural frequencies of the structure. VIV can be present in many engineering situations including marine and offshore applications such as in drilling and production risers. Due to its occurrence in diverse engineering applications, VIV has been the subject of extensive experimental and computational research including review articles in [1–5]. In studies of vortex-induced vibration, the physical model is usually a relatively long rigid or elastic cylinder placed normal to an incident uniform flow where the cylinder can vibrate transverse to the flow direction.

For a flexible and/or moving cylinder like a marine riser, the fluid interacts strongly with the riser motion and the vortex shedding frequency is captured by the body frequency over a wider range of flow speed [6]. Such a phenomenon is known as lock-in and the extent of the range of speed depends on the damping and mass of the riser [7]. Figure 1 presents a schematic sketch of three distinct branches obtained in experimental model of Khalak and Williamson [8].

The range of Reynolds number used here is 500–10000 which corresponds to the reduced velocity range of 0.5–10 and is included in the experimental data of [8]. The Steger and Warming [9] implicit factorization scheme is used to solve the RANS equations. The k-ε two equation turbulence model is used to simulate the turbulent flow in the wake. A similar computational study to duplicate the experimental results of [8] is reported by Wanderley and Levi [7]. The difference between the present numerical model with that of [7] is summarized in Table 1.

Table 1. Comparison of numerical models

	Present Model	Wanderley and Levi [7]
Turbulence Model	k-ε	Baldwin-Lomax
Numerical ‖Scheme	Steger-Warming	Beam-Warming
Factorization	Approximate	-------
Stretching Parameter	1.02	1.025

The numerical model used here is sufficiently accurate and robust and was able to duplicate experimental results of [8] with a success similar to

that achieved by [7], i.e., the Karman's vortex street effects on the lift and drag coefficients and the build-up and top part of the upper branch in Figure 1 were captured.
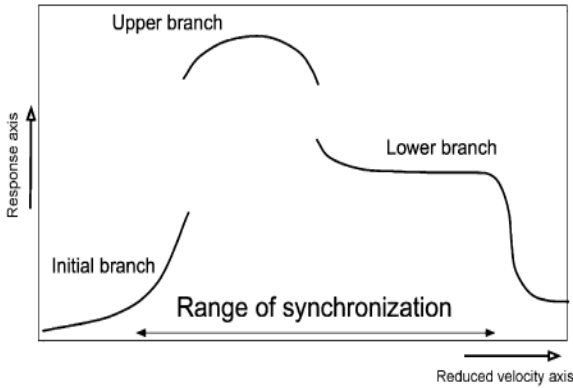

Figure 1. Sketch of three branches response model of Khalak and Willaimson (1996)

2. Governing Equations

The derivation of RANS equations in this section follows that of [7] closely. By breaking down the dependent variables into time averaged and varying parts, and also by using the mass-weighted averaging procedure of Farve [10] the RANS equations are derived. To present a general scheme of RANS equations, we first state them in a 3-D form although the simulations will be carried out in 2-D. Following the mass–weighted averaging procedure of Favre [10] the x-component of RANS equation can be written as follows:

$$\rho \left[\frac{\partial}{\partial x}(\overline{u}^2 + \overline{u'^2}) + \frac{\partial}{\partial y}(\overline{u}\,\overline{v} + \overline{u'v'}) + \frac{\partial}{\partial z}(\overline{u}\,\overline{w} + \overline{u'w'}) \right] = -\frac{\partial \overline{p}}{\partial x} \quad (1)$$

$$+ \mu \left[\frac{\partial^2 \overline{u}}{\partial x^2} + \frac{\partial^2 \overline{u}}{\partial y^2} + \frac{\partial^2 \overline{u}}{\partial z^2} \right]$$

This equation appears to be very similar to the steady-state, x-direction Navier-Stokes equation aside from terms involving the fluctuating velocities. It is conventional to transport these terms to the right-hand side so as to make the left-hand side b consistent with the steady state, Navier-Stokes x-direction equation:

$$\rho \left[\frac{\partial}{\partial x}(\overline{u}^2) + \frac{\partial}{\partial y}(\overline{u}\,\overline{v}) + \frac{\partial}{\partial y}(\overline{u}\,\overline{w}) \right] = -\frac{\partial \overline{p}}{\partial x} \quad (2)$$

$$+ \mu \left[\frac{\partial \overline{u}}{\partial x}(\mu \frac{\partial \overline{u}}{\partial x} - \rho \overline{u'^2}) + \frac{\partial \overline{u}}{\partial y}(\mu \frac{\partial \overline{u}}{\partial y} - \rho \overline{u'v'}) + \frac{\partial \overline{u}}{\partial z}(\mu \frac{\partial \overline{u}}{\partial y} - \rho \overline{u'w'}) \right]$$

The terms that appear in the last bracket of Eq. (1) are called Reynolds Stresses. This designation, while being traditional, is somewhat illogical because the terms in question arise from momentum flow rate terms. These "stresses" are the source that creates the turbulent disturbance of the otherwise steady Navier-Stokes equations. An often-cited form of the RANS equation:

$$\rho \left[\frac{\partial}{\partial x}(\overline{u}^2) + \frac{\partial}{\partial y}(\overline{u}\,\overline{v}) + \frac{\partial}{\partial y}(\overline{u}\,\overline{w}) \right] = -\frac{\partial \overline{p}}{\partial x}$$

$$+ \mu \left[\frac{\partial^2 \overline{u}}{\partial x^2} + \frac{\partial^2 \overline{u}}{\partial y^2} + \frac{\partial^2 \overline{u}}{\partial z^2} \right] - \left[\frac{\partial}{\partial x}(\overline{\rho u'^2}) + \frac{\partial}{\partial y}(\overline{\rho u'v'}) + \frac{\partial}{\partial z}(\overline{\rho u'w'}) \right]$$

(3)

Here the mass averaged parameters are obtained by following formula:

$$\tilde{f} = \frac{\overline{\rho f}}{\overline{\rho}} \quad (4)$$

The viscous stress tensor $\tilde{\tau}_{ij}$ can be written as follows:

$$\tilde{\tau}_{ij} = \mu \left[\left(\frac{\partial \tilde{u}_i}{\partial x_j} + \frac{\partial \tilde{u}_j}{\partial x_i} \right) - \frac{2}{3} \delta_{ij} \frac{\partial \tilde{u}_k}{\partial x_k} \right] \quad (5)$$

Writing the mean variables and the additional Reynolds stress terms such as indicated in Eq. (6), will yield the continuity and momentum terms of RANS equations.

$$\sigma_{ij} = -\overline{\rho u'_i u'_j} \quad (6)$$

Now, decomposing the components of the equation in two coordinate directions and considering the incompressible, turbulent momentum flow, the RANS equation can be written as follows:

$$\frac{\partial \tilde{u}}{\partial t} + \frac{\partial (\tilde{u}^2 + \overline{p}/\rho_\infty)}{\partial x} + \frac{\partial \tilde{u}\tilde{v}}{\partial y} + \frac{\partial \tilde{u}\tilde{w}}{\partial z} -$$

$$\frac{1}{\rho_\infty} \left[\frac{\partial \tilde{\tau}_{xx}}{\partial x} + \frac{\partial \tilde{\tau}_{xy}}{\partial y} + \frac{\partial \tilde{\tau}_{xz}}{\partial z} \right]$$

$$+ \frac{1}{\rho_\infty} \left[\frac{\partial \sigma_{xx}}{\partial x} + \frac{\partial \sigma_{xy}}{\partial y} + \frac{\partial \sigma_{xz}}{\partial z} \right] = 0 \quad (7)$$

$$\frac{\partial \tilde{v}}{\partial t} + \frac{\partial \tilde{u}\tilde{v}}{\partial x} + \frac{\partial (\tilde{v}^2 + \overline{p}/\rho_\infty)}{\partial y} + \frac{\partial \tilde{v}\tilde{w}}{\partial z} -$$

$$\frac{1}{\rho_\infty} \left[\frac{\partial \tilde{\tau}_{xy}}{\partial x} + \frac{\partial \tilde{\tau}_{yy}}{\partial y} + \frac{\partial \tilde{\tau}_{yz}}{\partial z} \right]$$

$$+ \frac{1}{\rho_\infty} \left[\frac{\partial \sigma_{xy}}{\partial x} + \frac{\partial \sigma_{yy}}{\partial y} + \frac{\partial \sigma_{yz}}{\partial z} \right] = 0 \quad (8)$$

$$\frac{\partial \tilde{w}}{\partial t} + \frac{\partial \tilde{u}\tilde{w}}{\partial x} + \frac{\partial \tilde{v}\tilde{w}}{\partial y} + \frac{\partial (\tilde{w}^2 + \overline{p}/\rho_\infty)}{\partial z} -$$

$$\frac{1}{\rho_\infty} \left[\frac{\partial \tilde{\tau}_{xz}}{\partial x} + \frac{\partial \tilde{\tau}_{yz}}{\partial y} + \frac{\partial \tilde{\tau}_{zz}}{\partial z} \right]$$

$$+ \frac{1}{\rho_\infty} \left[\frac{\partial \sigma_{xz}}{\partial x} + \frac{\partial \sigma_{yz}}{\partial y} + \frac{\partial \sigma_{zz}}{\partial z} \right] = 0 \quad (9)$$

To solve the RANS governing equations, the approximate factorization method, which is a stable approach in 2-D problems, is implemented. To estimate the convective terms and diffusion terms, the forward central difference and second order central difference schemes are used, respectively. Writing the RANS equation in 2–D curvilinear coordinates and in the conservative and dimensionless form will result in

a more convenient and straight forwarded shape of the equation as follows:

$$Q_t + (E_e - E_v)_\xi + (F_e - F_v)_\eta = 0 \tag{10}$$

where Q is the unknown vector, E and F are the flux vectors, and the subscript "*v*" is used to denote the viscous flux vectors. The transformed form of the vectors are presented as follows:

$$Q = \frac{1}{J}\begin{Bmatrix} p \\ u \\ v \end{Bmatrix}, E_e = \frac{1}{J}\begin{Bmatrix} pU \\ uU + p\xi_x \\ vU + p\xi_y \end{Bmatrix}, F_e = \frac{1}{J}\begin{Bmatrix} pV \\ uV + p\eta_x \\ vV + p\eta_y \end{Bmatrix} \tag{11}$$

$$E_v = \frac{1}{J}\left(\frac{1}{Re} + \mu_t\right)\begin{Bmatrix} 0 \\ A_1 u_\xi + A_2 u_\eta + A_3 v_\xi + A_4 v_\eta \\ A_3 u_\xi + A_5 u_\eta + A_6 v_\xi + A_7 v_\eta \end{Bmatrix} \tag{12}$$

$$F_v = \frac{1}{J}\left(\frac{1}{Re} + \mu_t\right)\begin{Bmatrix} 0 \\ A_2 u_\xi + A_{10} u_\eta + A_5 v_\xi + A_{11} v_\eta \\ A_4 u_\xi + A_{11} u_\eta + A_7 v_\xi + A_{12} v_\eta \end{Bmatrix} \tag{12}$$

$$Re = \frac{\rho_\infty U_\infty d}{\mu_\infty}$$

$$U = \xi_t + u\xi_x + v\xi_y \tag{13}$$

$$V = \eta_t + u\eta_x + v\eta_y$$

$$J = \xi_x \eta_y - \eta_x \xi_y$$

$$A_1 = \frac{4}{3}\xi_x^2 + \xi_y^2 \qquad A_6 = \xi_x^2 + \frac{4}{3}\xi_y^2$$

$$A_2 = \frac{4}{3}\xi_x \eta_x + \eta_y \xi_y \quad A_7 = \eta_x \xi_y + \frac{4}{3}\eta_y \xi_y$$

$$A_3 = \frac{\xi_x \xi_y}{3} \qquad\qquad A_{10} = \frac{4}{3}\eta_x^2 + \eta_y^2$$

$$A_4 = \eta_x \xi_y - \frac{2}{3}\eta_y \xi_x \quad A_{11} = \frac{\eta_x \eta_y}{3}$$

$$A_5 = \xi_x \eta_y - \frac{2}{3}\eta_x \xi_y \quad A_{12} = \eta_x^2 + \frac{4}{3}\eta_y^2 \tag{14}$$

Wanderley and Levi [7] used Baldwin-Lomax turbulent model to calculate the dynamic viscosity of modeled system. Here, the *k–ε* model [11], which is a two–equation turbulence model is used. The zero–equation models lack generality although they need minimum computer time, while two–equation models, have less limitations. As the boundary layer becomes separated, the zero–equation models are no longer relevant. As indicated in [12], the shear stress has qualitatively the same turbulent structure when it is detached as it is attached and the length scale is the height of the separated region. Here using this assumption, the *k–ε* model is based on eddy–viscosity concept given by:

$$v_t = C_\mu \frac{K^2}{\varepsilon} \tag{15}$$

where *Cμ* is a constant of dynamic turbulence and *K* and ε are obtained from differential equations representing transport of turbulence kinetic energy *K*,

and the rate of dissipation *ε*. The transport equations are:

$$\bar{u}\frac{\partial K}{\partial x} + \bar{v}\frac{\partial Y}{\partial y} =$$

$$\frac{\partial}{\partial y}\left(\frac{v_t}{\sigma_k}\frac{\partial K}{\partial y}\right) + v_t\left(\frac{\partial \bar{u}}{\partial y}\right)^2 - \varepsilon \tag{16}$$

$$\bar{u}\frac{\partial \varepsilon}{\partial x} + \bar{v}\frac{\partial \varepsilon}{\partial y} = \frac{\partial}{\partial y}\left(\frac{v_t}{\sigma_c}\frac{\partial \varepsilon}{\partial y}\right) +$$

$$C_{\varepsilon 1}\frac{\varepsilon}{K}v_t\left(\frac{\partial \bar{u}}{\partial y}\right)^2 - C_{\varepsilon 2}\frac{\varepsilon^2}{K} \tag{17}$$

The three terms on the right hand side of Eq. (16), are turbulent diffusion, turbulent energy production and viscous dissipation, respectively. The values of constants in the equations are given by [11]:
Cμ=0.09, *Cε1*=1.44, *Cε2*=1.92, *σk*=1.0, *σc*=1.3.
Considering three conditions of initial, boundary of the body surface and free stream boundary given in Eq. (18):

$$u = 1 \qquad v = 0 \qquad p = 1/M_\infty^2$$

$$u = 0 \qquad v = \dot{y} \qquad \partial p / \partial \eta = 0$$

$$u = 1 \qquad v = 0 \qquad p = 1/M_\infty^2$$

$$M_\infty = \text{practical range for incompressible flow} \tag{18}$$

The Eq. (11) is solved to obtain the flow variables. For the body motion equation, the dimensionless form of the Newton's second law for a cylinder can be written as follows:

$$\ddot{y} + C_\zeta \dot{y} + C_K y = \frac{C_L(Re)}{2C_\mu} \tag{19}$$

Where

$$C_\mu = \frac{m}{\rho D^2}, \quad C_K = \frac{4\pi^2}{U_r^2},$$

$$C_\zeta = \frac{4\pi\zeta}{U_r}, \quad U_r = \frac{U}{f_n d}$$

and subscripts *L*, *k* and *ζ* are used to denote lift, stiffness and damping coefficients, respectively, and $y, \dot{y}, \ddot{y}$ are displacement, velocity and acceleration of the riser. The initial conditions are:

$$y(0) = 0, \quad \dot{y}(0) = 0 \tag{20}$$

3. Numerical formulation
A simple algebraic grid generator method (using geometrical progression) is used to generate the computational space around the riser. To capture more information at area adjacent to the wall, the stretching parameter of q=1.02 is used. In [7] this parameter is equal to 1.025. Then the RANS and body motion equations were solved simultaneously, to obtain C_L and in turn the position of riser. To obtaining the C_L coefficient an integration of pressure and skin friction distribution around the riser surface is conducted. The pressure distribution is obtained in the previous RANS formulation. The governing equations were solved as follows:

3.1. RANS equation

Eq.(10) can be written in the implicit form as follows:

$$\frac{Q^{n+1} - Q^n}{\Delta\tau} + \left(\frac{\partial E}{\partial\xi}\right)^{n+1} + \left(\frac{\partial F}{\partial\eta}\right)^{n+1}$$

$$- \left(\frac{\partial E_v}{\partial\xi}\right)^{n+1} - \left(\frac{\partial F_v}{\partial\eta}\right)^{n+1} = 0$$

$$(21)$$

Since the scheme of solution is implicit, a linearization procedure is applied to the RANS equation. The linearization can yield efficient and more accurate results. So, a linearization process was applied on RANS equations in present study. Using the Taylor series, the viscous and inviscid flux vectors appeared in the left hand side of Eq. (21), can be written based on the Jacobin matrices of A, B, A_v and B_v (gradients of flux vectors with respect to the variable vector, Q) in the following form:

$$\frac{\Delta Q}{\Delta\tau} + \frac{\partial}{\partial\xi}\left(E^n + A\Delta Q\right) + \frac{\partial}{\partial\eta}\left(F^n + B\Delta Q\right)$$

$$- \frac{\partial}{\partial\xi}\left(E_v^{\,n} + A_v\Delta Q\right)$$

$$- \frac{\partial}{\partial\eta}\left(F_v^{\,n} + B_v\Delta Q\right) = 0$$

$$(22)$$

which can be rewritten as follows:

$$\left\{ I + \Delta\tau\left[\frac{\partial}{\partial\xi}(A) + \frac{\partial}{\partial\eta}(B) - \frac{\partial}{\partial\xi}(A_v) - \frac{\partial}{\partial\eta}(B_v)\right]\right\}\Delta Q =$$

$$- \Delta\tau\left[\frac{\partial E^n}{\partial\xi} + \frac{\partial F^n}{\partial\eta} - \frac{\partial E_v^n}{\partial\xi} - \frac{\partial F_v^n}{\partial\eta}\right]$$

$$(23)$$

where I is the identity matrix. To increase the efficiency of solution of Eq.(23), the approximate factorization was applied. This procedure has reduced the process time of the developed code considerably. It converts the block penta-diagonal system of equations to a block three-diagonal system, which is more efficient and has potential to prevent expensive mathematical computations. Approximate factorization may create some instability in 3-D problems and may need artificial dissipation but it is quite stable for 2-D problems. In addition by splitting the Jacobin matrices based on their eigenvalues, the following two step form of equation can be obtained:

$$\left[I + \Delta\tau\frac{\partial}{\partial\xi}(A^+ + A^-) - \Delta\tau\frac{\partial A_v}{\partial\xi}\right]\Delta Q^* =$$

$$- \Delta\tau\left[\frac{\partial}{\partial\xi}(E^+ + E^-) + \frac{\partial}{\partial\eta}(F^+ + F^-) - \frac{\partial E_v}{\partial\xi} - \frac{\partial F_v}{\partial\eta}\right]$$

$$(24)$$

And

$$\left[I + \Delta\tau\frac{\partial}{\partial\eta}(B^+ + B^-) - \Delta\tau\frac{\partial B_v}{\partial\eta}\right]\Delta Q = \Delta Q^*$$

$$(25)$$

Simplifying the above equations and introducing the central difference approximation to inviscid terms, the compact forms of equations can be written as follows:

$$CAM = -\left[\frac{\Delta\tau}{\Delta\xi}A_{i-1j}^+ + \frac{\Delta\tau}{2\Delta\xi^2}\hat{r}_{i-1j}R_{i-1j}\right]$$

$$CA = \left[I + \frac{\Delta\tau}{\Delta\xi}\left(A_{ij}^+ + A^-_{ij}\right) + \frac{\Delta\tau}{2\Delta\xi^2}\hat{r}_{ij}R_{ij}\right]$$

$$CAP = \left[\frac{\Delta\tau}{\Delta\xi}A_{i+1j}^- - \frac{\Delta\tau}{2\Delta\xi^2}\hat{r}_{i+1j}R_{i+1j}\right]$$

$$CBM = -\left[\frac{\Delta\tau}{\Delta\eta}B_{ij-1}^+ + \frac{\Delta\tau}{2\Delta\eta^2}\hat{s}_{ij-1}S_{ij-1}\right]$$

$$CB = \left[I + \frac{\Delta\tau}{\Delta\eta}\left(B_{ij}^+ - B_{ij}^-\right) + \frac{\Delta\tau}{2\Delta\eta^2}\hat{s}_{ij}S_{ij}\right]$$

$$CBP = \left[\frac{\Delta\tau}{\Delta\eta}B_{ij+1}^- - \frac{\Delta\tau}{2\Delta\eta^2}\hat{s}_{ij+1}S_{ij+1}\right]$$

$$RHS = -\Delta\tau\left\{\begin{array}{l}\frac{1}{\Delta\xi}\left(E_{ij}^+ - E_{i-1j}^+ + E_{i+1j}^- - E_{ij}^-\right) + \frac{1}{\Delta\xi}\left(F_{ij}^+ - F_{ij-1}^+ + F_{ij+1}^- - F_{ij}^-\right) \\ -\frac{1}{2\Delta\xi^2}\left[\hat{e}_{i+1j}\hat{E}_{i+1j} - \hat{e}_{ij}\hat{E}_{ij} + \hat{e}_{i-1j}\hat{E}_{i-1j}\right] \\ -\frac{1}{2\Delta\eta^2}\left[\hat{f}_{ij+1}\hat{F}_{ij+1} - \hat{f}_{ij}\hat{F}_{ij} + \hat{f}_{ij-1}\hat{F}_{ij-1}\right]\end{array}\right\}$$

where r, s, e, f and corresponding capital letters, are functions of constants of Eqs. (24-25). Finally, by the Steger and Warming implicit scheme the RANS equations can be written as the following two equations:

$$CAM_{ij}\Delta Q_{i-1j}^{\,*} + CA_{ij}\Delta Q_{ij}^{\,*} + CAP_{ij}\Delta Q^*_{i+1j} = RHS_{ij}$$

$$(26)$$

$$CBM_{ij}\Delta Q_{ij-1} + CB_{ij}\Delta Q_{ij} + CBP_{ij+1}\Delta Q_{ij+1} = \Delta Q^*_{ij}$$

$$(27)$$

3.2. Body motion equation

To solve the body motion equation, two explicit methods were used. From Eq.(19), the acceleration term can simply be written as:

$$\ddot{y}^n = \frac{C_L^n}{2C_\mu} - C_\zeta\dot{y}^n - C_K y^n$$

$$(28)$$

Applying the Lax–Wendroff and Euler methods, the position and velocity of riser can be obtained as follows:

$$\dot{y}^{n+1} = \dot{y}^n + \ddot{y}^n\Delta t$$

$$(29)$$

$$y^{n+1} = y^n + \dot{y}^n\Delta t + \frac{1}{2}\ddot{y}^n\Delta t^2$$
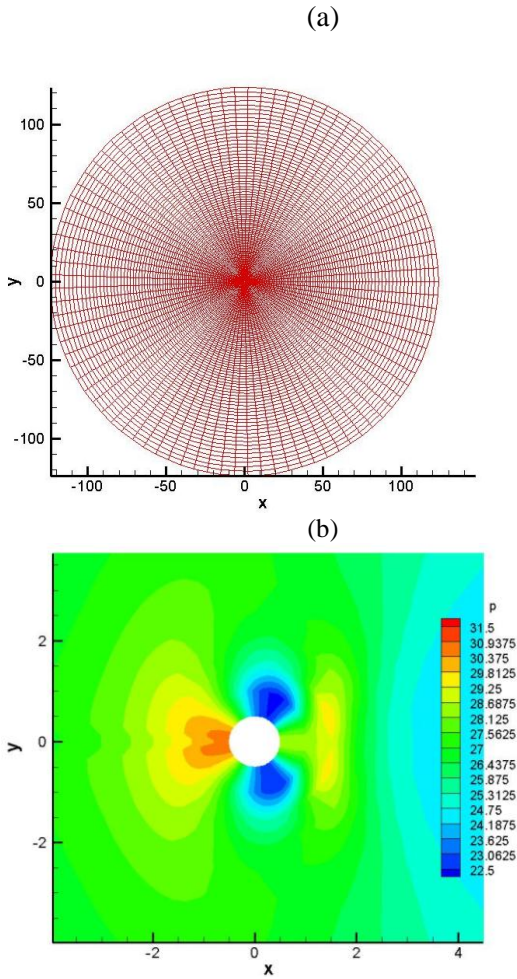
$$(30)$$

4. Results and Discussion

Results of the work and discussions are presented here. First, the laminar flow results for *Re=100* are compared with other results presented in the literature. Fig 2 shows the generated grid in the physical domain. In order to compare the results with those of Wanderley and Levi [7] a distance to free stream equal to 120 times of cylinder diameter is considered. Although this configuration increases the data points and the computational time, it ensures capturing the properties of vortices in long distances and all possible regions. Table 2 compares results of the present numerical model with other numerical and experimental results in the literature for the lift coefficient. The higher value of lift coefficient

obtained in the present model, could be related to the special finite difference scheme used here. However, the main reason of overestimation of C_L needs more investigations in future works.

(a)

(b)

Fig. 2 (a): Computational grid in the physical domain. (b): Pressure contours around a circular cylinder for Re=100;

The present model, failed to improve the computation time. The time required for computation of eigenvalues of Jacobin matrices in the Steger–Warming formulation, may be the main reason for the high computational time.

Figure 3 shows the variation of lift force as a function of time at *Re=100*. As can be seen, numerical modeling of the phenomenon is able to present the real picture of the flow physics, since the oscillation in lift force is caused by the variation of pressure in effect of alternating vortex shedding in the wake of the riser. Fig. 4 shows the alternating nature of the vortices in four distinct time steps at *Re=100*. The

well-known vortex street of Karman is quite obvious at this figure.

Table 2. Comparison between results obtained by the present work and other numerical and experimental data

Reference	Trriton [15] (dt=0.005)	Herfjord [14]	J.B. Wanderley [7]	Present study (dt=0.004)
Model type	experimental	Finite element	Finite difference (Beam-Warming)	Finite difference (Steger - Warming)
Reynolds no	100	100	100	100
Lift coefficient	0.34	0.34	0.313	0.37

Fig. 3 Time variation of lift force at Re=100

After the accuracy of the model is verified at *Re=100*, the modeling was generalized to other Reynolds numbers. The Reynolds numbers used in the present study are in the range of 500 to 10000 which are proportional to the reduced velocity in the range of 0.5 to 10. The mass and damper coefficients used here, were *Cμ=1.88* and *ζ=5.42×10-3*, which are the same coefficients used in [7] and [8]. Fig. 5 shows results obtained for the transversal displacement of the vibrating circular cylinder as a function of time. The time is traced in two states, one in the build-up of the upper branch and another at the top of the upper branch Khalak and Williamson [8]. Two values of reduced velocities of *Ur=4.5* in Fig. 5a and *Ur=6.5* in Fig. 5b correspond to the build-up and top part of the upper branch, respectively. The main reason that the lower branch in fig. 1 was not captured at present model may be related to the 2-D modeling using RANS equations, while the lower branch has been obtained in experimental model of Khalak and Williamson [8] which is 3-D.
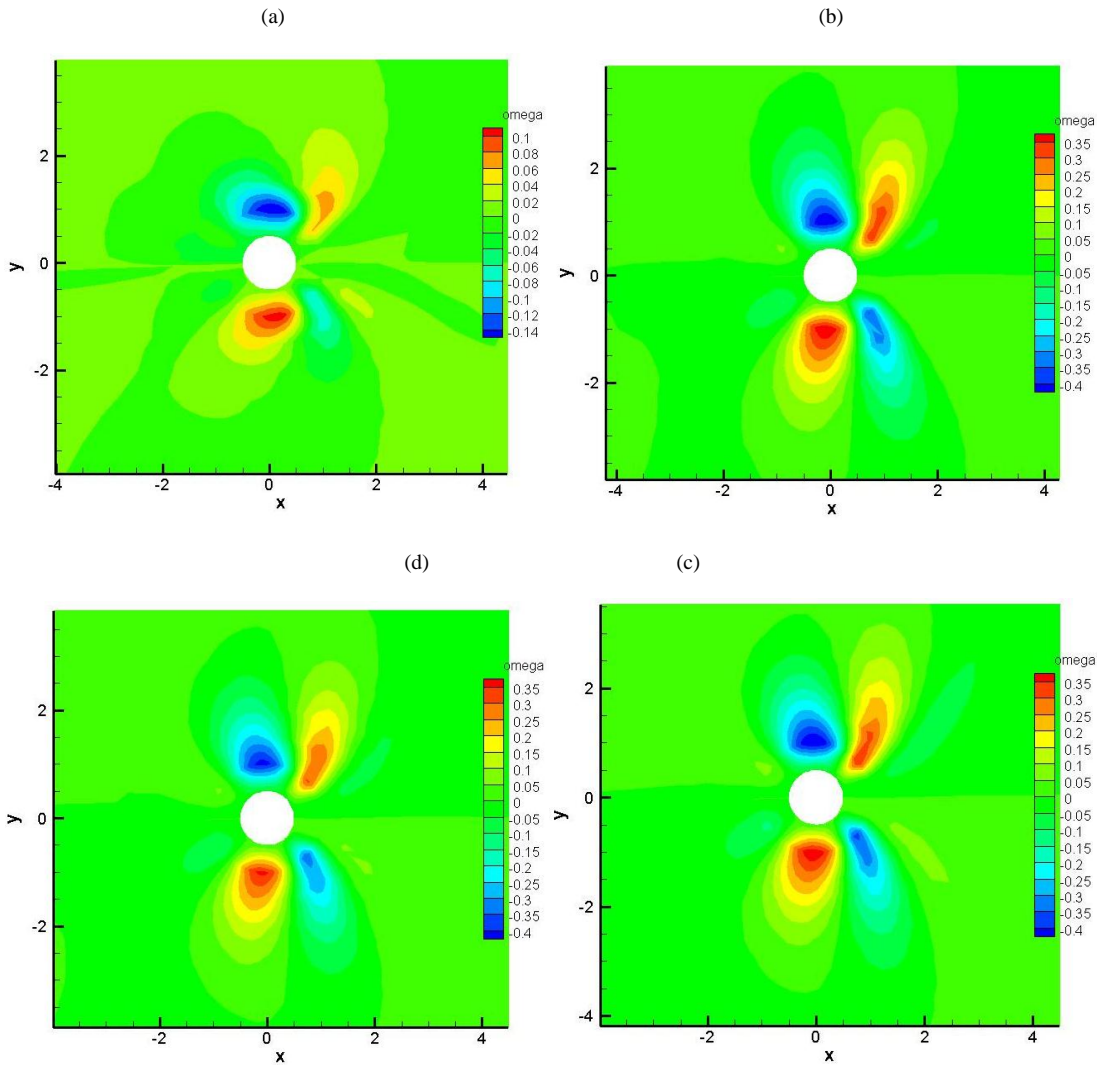
5

(a)

(b)

(d)

(c)

Fig. 4 Vortex strength contours at Re=100 in four time steps: (a) 100, (b) 500, (c) 1000, (d) 5000
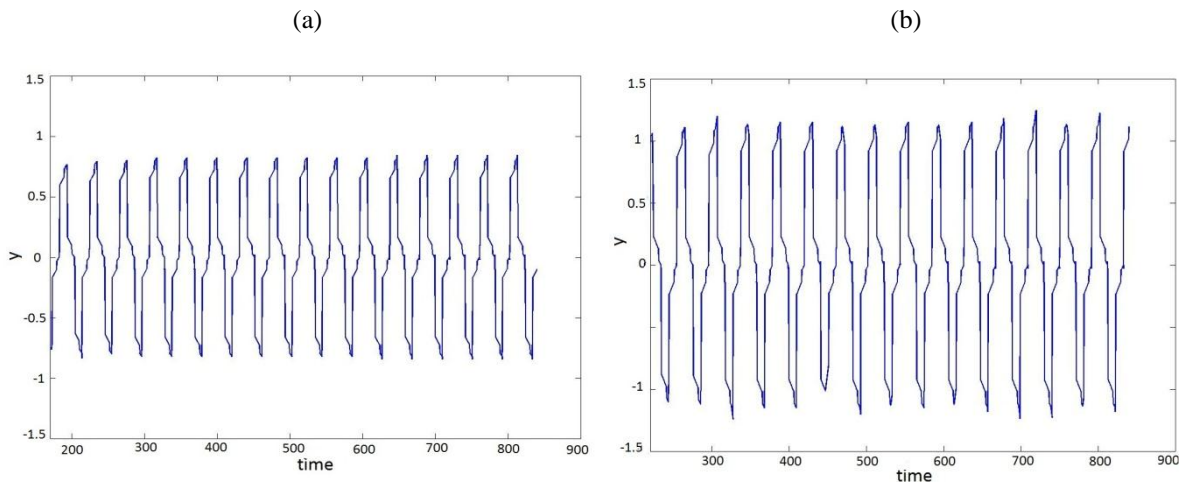
(a)

(b)

Fig. 5 Transversal displacement of the riser for (a) Ur=4.5; (b) Ur=6.5.

The main reason the displacement is greater for U_r=6.5 than U_r=4.5 is that U_r=6.5 is in the lock–in region, i.e. the region of top part of upper branch in Figure 1, where the synchronization of frequencies occurs. Figure 6 shows the spectral analysis of displacements for U_r=6.5. As seen, the main component of period of displacements is lied on T=39.81s which justify entering riser to lock–in area

at that reduced velocity, since this time period is very close to the natural period of riser displacement (T_n=40s). The features presented here are in close agreement with those presented in Khalak, and Williamson [8].
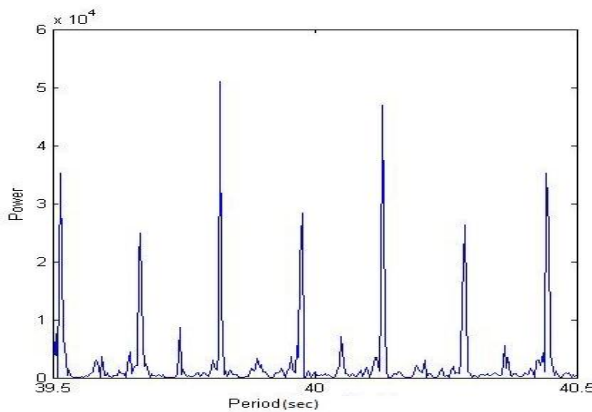
Fig. 6 Spectral analysis of riser displacement, U_r=6.5 (Re=6500)

5. Conclusions

Vortex-Induced vibration is a major concern in offshore oil and gas industry. This phenomenon can cause considerable damage to production lines. Here, a numerical code was developed to capture the vibration ranges of the risers and the comparison of the results show that the finite difference method can be considered as an efficient model tool to simulation of riser dynamics. Is is also indicated that the regime of so called the riser wake can also be captured using the present finite difference method.

First, the results were obtained at *Re=100*, and compared by data available in the literature. Then the solution was generalized to other *Re* (or *Ur*) values. The present mathematical model and respective numerical formulation were able to capture the upper branch of the amplitudes of oscillation reported in Khalak, and Williamson [8]. The lower branch obtained in the present investigation did not agree with the experimental data. To modeling this part of riser oscillation, it is needed to more robust models such 3-D ones to obtain an accurate results for lower branch regime.

The main features of present numerical investigation are:

- Using the *k-ε* turbulent model which is more suitable for separated flows.
- Formulating the conservative form of governing equations
- Applying the approximate factorization to increase the efficiency of solution.

Further investigations can include studying the problem with other turbulence models in CFD. Using the three-dimensional simulation and considering the more complicated geometries of the riser using overlapping Chimera Multi-block grids Houzeaux and Codina [13].

6. References

1- Griffin, O.M., and Ramberg, S.E., (1982), *Some recent studies of vortex shedding with application to marine tubular sand risers*. ASME Journal of Energy Resource Technology Vol.104, p.2–13.

2- Bearman, P.W., (1984), *Vortex shedding from oscillating bluff bodies*. Annual Review of Fluid Mechanics Vol.16, p.195–222.

3- Parkinson, G., (1989), *Phenomena and modeling of flow-induced vibrations of bluff bodies*. Progression Aerospace Sciences Vol.26, p.169–224.

4- Sarpkaya, T., (2004), *A critical review of the intrinsic nature of vortex-induced vibrations*, Journal of Fluids and Structures 1Vol.9, p.389–447.

5- Williamson, C.H.K., and Govardhan, R., (2004), *Vortex-induced vibrations,* Annual Review of Fluid Mechanics, Vol.36, p.413–455.

6- Bearman, P.W., (2000), *Developments in Vortex Shedding Research, Workshop on Vortex-Induced Vibrations of Offshore Structures*. Sao Paulo, Brazil.

7- Wanderley J.B., and Levi, C., (2005), *Vortex induced loads on marine risers*, Ocean Engineering Vol.32, p.1281–1295.

8- Khalak, A., and Williamson, C.H.K., (1996) *Dynamics of a hydroelastic cylinder with very low mass and damping*. Journal of Fluids and Structures, Vol.10, p.455–472.

9- Steger, J.L., and Warming, R.F, (1979), *Flux vector splitting of invicid gas dynamic equations with application to finite difference method*. NASA. TM-78605.

10- Favre, A., (1965) *Equations des gaz turbulents compressibles*: 1 Formes Ge´ne´rales. Journal of Mechanics, Vol.4, p.361–390.

11- Jones W.P., and Launder, B.E., (1997), *The prediction of relaminarization with a two-equation model of turbulence*, International Journal of Heat and Mass Transfer, Vol.15, p.301-314.

12- Goldberg, U.C., (1986), S*eparated flow treatment with a new turbulence model*, AIAA Journal, Vol.24(10), p. 1711-1713.

13- Houzeaux, G., and Codina, R., (2003), *A chimera method on a Dirichlet/Neumann (Robin) coupling for the Navier—Stokes equations*. Computational Methods Application and Mechanical Engineering, Vol.192, p.3343–3377.

14- Herfjord, K., (1995), *A study of two-dimensional separated flow by a combination of the finite element method and Navier–Stokes Equations*, Dr. Eng. Theses, The Norwegian Institute of Technology, Trondheim, Norway.

15- Tritton, D.J., (1959), *Experiments on the flow past a circular cylinder at low Reynolds number*, Journal of Fluid Mechanics, Vol.6, p.